Geometrical Control of Active Turbulence in Curved Topographies

D. J. G. Pearce, Perry W. Ellis, Alberto Fernandez-Nieves, and L. Giomi

Phys. Rev. Lett. **122**, 168002 — Published 26 April 2019

DOI: 10.1103/PhysRevLett.122.168002

Geometrical control of active turbulence in curved topographies

D. J. G. Pearce,[1] Perry W. Ellis,[2] Alberto Fernandez-Nieves,[2,3,4,*] and L. Giomi[1,†]

[1] *Instituut-Lorentz, Universiteit Leiden, P.O. Box 9506, 2300 RA Leiden, The Netherlands*
[2] *School of Physics, Georgia Institute of Technology, Atlanta, Georgia 30332, USA*
[3] *Department of Condensed Matter Physics, University of Barcelona, 08028 Barcelona, Spain*
[4] *ICREA-Institucio Catalana de Recerca i Estudis Avancats, 08010 Barcelona, Spain*

We investigate the turbulent dynamics of a two-dimensional active nematic liquid crystal constrained on a curved surface. Using a combination of hydrodynamic and particle-based simulations, we demonstrate that the fundamental structural features of the fluid, such as the topological charge density, the defect number density, the nematic order parameter and defect creation and annihilation rates, are approximately linear functions of the substrate Gaussian curvature, which then acts as a control parameter for the chaotic flow. Our theoretical predictions are then compared with experiments on microtubule-kinesin suspensions confined on toroidal active droplets, finding excellent qualitative agreement.

Experimental studies on active liquid crystals [1–19] have opened, in the past decade, a Pandora's box of novel hydrodynamic phenomena with no counterparts in passive complex fluids. Active liquid crystals are orientationally ordered fluids consisting of self- or mutually-propelled rod-shaped constituents, generally of biological origin. Examples include *in vitro* mixtures of microtubules and kinesin [1–4, 6–8], actomyosin gels [9, 10], suspensions of motile cells, such as flagellated bacteria [11–16] and sperm [17, 18], and "living liquid crystals" [19]. Depending on the abundance of biochemical fuel as well as the system density and geometry, these active liquids have been observed to self-organize into an extraordinary variety of spatiotemporal patterns, including traveling bands [9] and vortices [16], oscillating textures [4, 9], ordered arrangements of topological defects [6, 17] and turbulent flows at low Reynolds number [2, 11, 12, 14, 15, 18, 19].

Starting from the pioneering work by Keber *at al.* [4] on active nematic vesicles, unraveling the interplay between substrate geometry and the collective motion of active fluids has surged as one of the fundamental challenges in the physics of active materials. In spite of the variety of interesting phenomena discussed in the literature [20, 21] and with special emphasis in the case of spherical active fluids [4, 22–25], a coherent theoretical picture, which accounts for the threefold coupling between substrate geometry, orientational dynamics and hydrodynamic flow, is still lacking.

In a recent work, we have investigated the dynamics of a turbulent active nematic suspension of microtubules and kinesin confined on a toroidal droplet [5]. Using a combination of experiments and a Coulomb gas model of active defects [26–28], we demonstrated that, because of passive elastic interactions [29, 30], defects in active nematics are sensitive to the Gaussian curvature of the substrate. As turbulence progresses toward fully developed, this effect becomes weaker and weaker, but never completely disappears. However, the Coulomb gas model abstracts the full active nematic to a collection of point particles, thus providing no information on the effect of the hydrodynamic flow, beside the active propulsion of the defects.

In this Letter we overcome this limitation and generalize the hydrodynamic theory of active nematics to arbitrarily curved substrates. By focusing on the fully developed turbulent regime, we demonstrate that topological defects can be controlled through the substrate geometry. For the specific case of axisymmetric tori, we show that this behavior originates from the interplay between passive elastic interactions, driving the defects toward regions of like-sign Gaussian curvature, and active hydrodynamical effects, which result into a a non-uniform defect-creation rate. Finally, we compare our predictions with experiments on microtubule-kinesin suspensions confined to toroidal active droplets, finding excellent qualitative agreement.

Let $\boldsymbol{r} = \boldsymbol{r}(x^1, x^2)$ be the position of generic surface embedded in $\mathbb{R}^3$ and parametrized by the coordinates (x^1, x^2). Furthermore, let $\boldsymbol{g}_i = \partial_i \boldsymbol{r}$ be a basis of covariant vectors on the tangent plane, so that $g_{ij} = \boldsymbol{g}_i \cdot \boldsymbol{g}_j$ is the surface metric tensor. A configuration of an active nematic monolayer constrained to lie on the surface can be described in terms of the local velocity field $\boldsymbol{v} = v^i \boldsymbol{g}_i$ and nematic tensor $\boldsymbol{Q} = Q^{ij} \boldsymbol{g}_i \boldsymbol{g}_j$, where

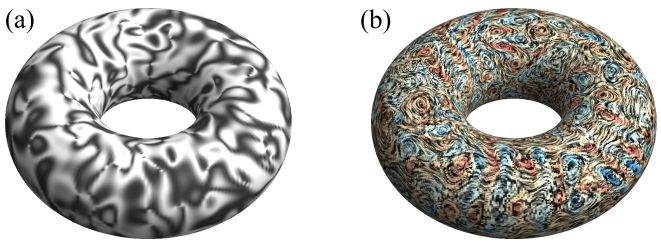

FIG. 1. (a) Schlieren texture and (b) flow on a toroidal active nematic obtained from a numerical integration of Eqs. (1). Dark regions correspond to local configurations of the director parallel or perpendicular to the meridians of the torus, while red (blue) indicate regions of positive (negative) vorticity.

$Q^{ij} = S(n^i n^j - g^{ij}/2)$, with S the nematic order parameter and $\boldsymbol{n} = n^i \boldsymbol{g}_i$ the nematic director, such that $n^i n_i = 1$. Incompressibility requires $\nabla_i v^i = 0$, with ∇_i the covariant derivative. The hydrodynamic equations governing the evolution of the active nematic fluid of density ρ and viscosity η can be expressed in covariant form as follows [31]:

$$\rho \frac{Dv^i}{Dt} = \eta(\Delta_{\rm B} + K)v^i - \nabla^i P - \zeta v^i + \alpha \nabla_j Q^{ij} \ , \quad \text{(1a)}$$

$$\frac{DQ^{ij}}{Dt} = \frac{\lambda}{2} S u^{ij} - \frac{1}{2}\omega(\epsilon^i_k Q^{kj} + \epsilon^j_k Q^{ki}) + \frac{1}{\gamma} H^{ij} \ , \quad \text{(1b)}$$

where $D/Dt = \partial_t + v^k \nabla_k$ is the covariant material derivative, $\Delta_{\rm B} = g^{ij}\nabla_i \nabla_j$ is the covariant (or Bochner) Laplacian and P the pressure. The term $\eta K v^i$, with K the Gaussian curvature, represents the additional shear force arising from the fact that streamlines inevitably converge or diverge on surfaces with non-zero Gaussian curvature, whereas $-\zeta v^i$, with ζ a friction coefficient, is the damping force arising form the possible interaction with the external environment. The last term in Eq. (1a) arises from the divergence of the active stress $\boldsymbol{\sigma}^{\rm a} = \alpha \boldsymbol{Q}$, where the constant α embodies the biochemical activity of the system. In Eq. (1b), λ is the flow-alignment parameter, $u^{ij} = (\nabla^i v^j + \nabla^j v^i)/2$ is the strain-rate tensor, $\omega = \epsilon_{ij}\nabla^i v^j$ is the vorticity, with ϵ_{ij} the anti-symmetric Levi-Civita tensor and $\epsilon^j_i = g^{ik}\epsilon_{jk}$, γ is the rotational viscosity and $H^{ij} = -\delta F/\delta Q^{ij}$ is the molecular tensor describing the orientational relaxation of the system, with F the free-energy. Following Kralj *et al.* [32], we express F as:

$$F = \int \mathrm{d}A \left[\frac{a_2 t}{2} Q_{ij}Q^{ij} + \frac{a_4}{4}(Q_{ij}Q^{ij})^2 + \frac{k}{2}\nabla_i Q_{jk}\nabla^i Q^{jk} - \frac{k_{24}}{2} K Q_{ij}Q^{ij} + k_e Q_{ij} K^{jk} K^i_k \right] , \quad (2)$$

where a_2 and a_4 are constants, t is the reduced temperature and is negative in the nematic phase, $K_{ij} = -\boldsymbol{g}_i \cdot \partial_j \boldsymbol{N}$, with $\boldsymbol{N}$ the normal vector, is the extrinsic curvature tensor and k, k_{24} and k_e are phenomenological elastic constants detailing the cost of distortions in $\boldsymbol{Q}$, the cost of forming an ordered phase where $K \neq 0$ and the coupling between the order and the extrinsic curvature, respectively [33–35].

Eqs. (1) describe the dynamics of an active nematic monolayer on a generic curved surface. To provide an example and make contact with experiments, we have considered the specific case of an active nematic constrained on an axisymmetric torus (Fig. 1). Unlike the sphere, the torus is a closed surface having non-uniform Gaussian curvature. The latter is positive and maximal on the outer equator, negative and minimal on the inner equator and varies smoothly over the surface, resulting into a vanishing Euler characteristic: $\chi = 1/(2\pi)\int K \, \mathrm{d}A = 0$. When a torus is coated with a nematic liquid crystal, this property implies global topological charge neutrality: i.e. $\sum_n s_n = 0$, with s_n the topological charge, defined as the winding number of the nematic director along a path encircling the $n-$th defect. In practice, $s_n = \pm 1/2$, due to the prohibitive energetic cost of higher-charge disclinations in two dimensions [5].

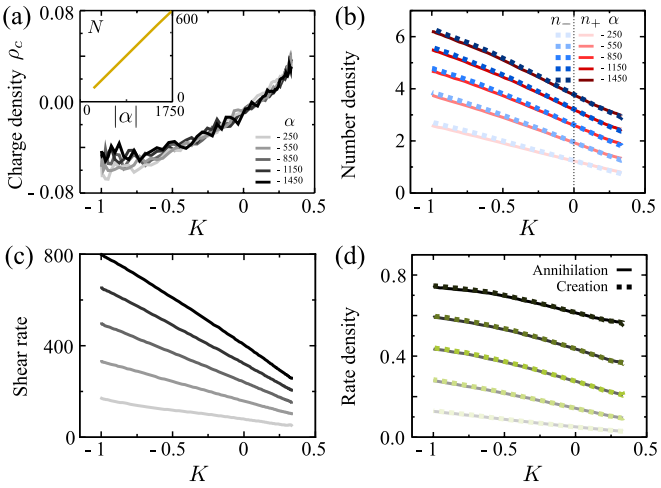

FIG. 2. Structural properties of toroidal active nematics versus Gaussian curvature, obtained from a numerical integration of Eqs. (1). (a) Topological charge density ρ_c. When turbulence is fully developed, increasing the activity has little effect on ρ_c, but causes a linear increase in the number of defects (inset). (b) Number density of $+1/2$ (n_+) and $-1/2$ (n_-) disclinations. In contrast to passive liquid crystals on curved surfaces, both densities are larger in the interior of the torus, where the Gaussian curvature is negative. (c) Annihilation and creation rate densities are both increased in the interior of the torus. (d) Shear-rate $u^{\theta\phi}$, with θ and ϕ the coordinates along the meridian and parallel respectively. All quantities are rescaled as explained in the main text.

Eqs. (1) have been numerically integrated using the vorticity/stream-function approach [31]. To make Eqs. (1) dimensionless, we rescale length by the cross-sectional radius of the torus, b, time by the relaxational time scale $k/(\gamma b^2)$ of the $\boldsymbol{Q}-$tensor and mass by ρb^2. In these units, we set $k = 1$, $k_e = 0$, $k_{24} = 0$, $\eta = 0.1$, $\zeta = 0.1$ and $\lambda = 0.5$. The torus aspect ratio is $\xi = a/b = 2$, with a the radius of the central ring.

Figs. 1a,b illustrate a typical configuration of the nematic director and the vorticity. As in the case of a flat substrate, active nematics are found in a turbulent regime when the active length scale $\ell_{\rm a} = \sqrt{k/|\alpha|}$, resulting from the balance between active and passive stresses [36], is much smaller than the torus cross-sectional radius b and the frictional screening length $\ell_{\rm f} = \sqrt{\eta/\zeta}$. In this regime, the flow is organized in vortices of average size $\ell_{\rm a}$ and the director is decomposed in domains surrounded by $\pm 1/2$ disclinations. While on the plane these structures are uniformly distributed, Fig. 1 shows a higher den-

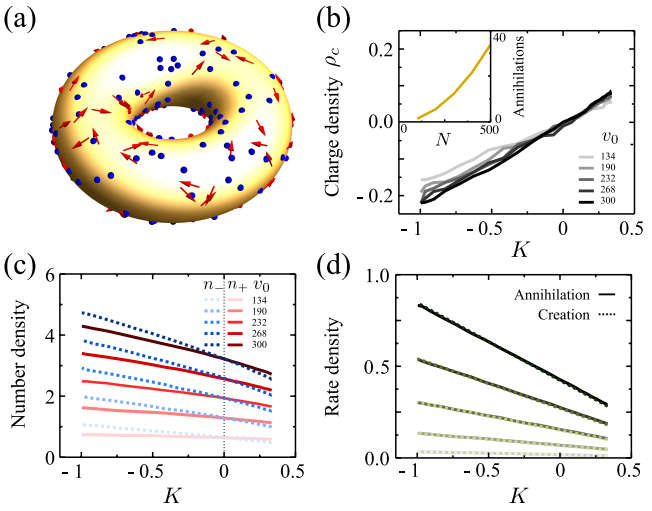

FIG. 3. Structural properties of toroidal active nematics versus Gaussian curvature, obtained from the Coulomb gas model, Eqs. (3). In all plots, length is rescaled by the cross-sectional radius b, time by $b^2/(\mu k)$ and velocity by $\mu k/b$. Activity is controlled by simultaneously varying the dimensionless defect velocity v_0 and the number N, taking advantage of the fact that $v_0 \sim \sqrt{\alpha}$ and $N \sim \alpha$ (Fig. 2a inset). Specifically, we set $v_0 = 6\sqrt{500/N}$. (a) Snapshot of a typical configuration (b) Topological charge density versus Gaussian curvature for varying v_0 and N. (Inset) The number of annihilations scales quadratically with the number of defects, hence with α. (c) Number density of $+1/2$ (n_+) and $-1/2$ (n_-) disclinations. (d) The annihilation and creation rate density. In all simulations, $\zeta_n^r = 0.1$ and $|\boldsymbol{\zeta}_n^t| = 0.1$ in the units described above.

sity of vortices in the interior of the torus. These simple observations already suggest a correlation between the substrate geometry and the spatial organization of the coherent structures emerging within the active flow. In order to quantify this effect we have measured the time-averaged topological charge density ρ_c of the defects as a function of the Gaussian curvature K (Fig. 2a). We find that ρ_c increases monotonically with K and attains its largest magnitudes along the equators. This behavior originates from the elasticity of the nematic phase. Assuming the nematic order parameter constant outside the core of the defects, Eq. (2) approximates the one-elastic-constant Frank free-energy. In the presence of a distribution of topological defects, the latter is given by $F_{\rm F} = k/2 \int {\rm d}A\, |\nabla\varphi|^2$ [29, 30], with φ a *geometric potential* given by $\Delta_{\rm LB}\varphi = \rho_c - K$, with $\Delta_{\rm LB}$ the Laplace-Beltrami operator [31]. This implies that the lowest energy state is attained when $\rho_c = K$ and $\varphi = $ const. Although in the turbulent regime investigated here the system is well away from its lowest free energy state, topological defects are still subject to elastic forces attracting them to regions of like-sign Gaussian curvature, thus $\rho_c \sim K$.

This result is consistent with prior experiments and numerical simulations using a Coulomb gas model [5], and can be understood based on the mechanical properties of nematic liquid crystals at equilibrium. Hydrodynamics, however, enables us to go beyond this and shed light on the non-equilibrium nature of defect proliferation. Fig. 2b shows the number density $n_\pm$ of positive (solid line) and negative (dashed line) defects, such that $\rho_c = (n_+ - n_-)/2$. Both densities are essentially linear function of K but, surprisingly, both have negative slope. This implies that positive defects are denser in the negative Gaussian curvature region, in direct contrast to the passive case, in which the positive defects are only found in the positive Gaussian curvature region [37, 38]. At $K = 0$, n_+ and n_- crossover, so that, at $K = 0$, the topological charge density vanishes, as observed in Fig. 2a. This beahvior is, in turn, correlated with the configuration of the shear-rate (Fig. 2c) and the defects creation/annihilation rate (Fig. 2d), that are both monotonically decreasing with the distance from the inner equator of the torus.

Given that the passive elastic forces always drive the positive defects towards the regions of positive Gaussian curvature, the increased density of the positive defects in regions of negative K must originate from non-equilibrium effects. We conjecture that the higher normal curvature in the interior of the torus results into a higher shear-rate in the flow (Fig. 2c), which, in turn, leads to a stronger distortion of the nematic director and a larger defect creation rate (Fig. 2d). On the other hand, the geometrical forces due to the Gaussian curvature biases the positive (negative) topological charge toward the exterior (interior) of the torus, but, because of the short mean-free path of the defects, this does not lead to a complete segregation of the topological charge. As a consequence, the density of both positive and negative defects is larger in the interior of the torus, although their difference is proportional to K.

To test this hypothesis, we use a variant of the Coulomb gas model of active nematic defects [4, 5, 26–28], augmented with a non-uniform defect creation distribution reproducing the outcome of the hydrodynamic simulations. Defects are modelled as massless particles on the torus, whose position $\boldsymbol{r}_n$ and orientation $\boldsymbol{p}_n$ are governed by the following equations of motion:

$$\frac{{\rm d}\boldsymbol{r}_n}{{\rm d}t} = v_0\boldsymbol{p}_n + \mu\boldsymbol{F}_n + \boldsymbol{\zeta}_n^t\,, \qquad \frac{{\rm d}\boldsymbol{p}_n}{{\rm d}t} = \zeta_n^r\boldsymbol{p}_n^\perp\,, \quad (3)$$

where v_0 is the speed at which defects are propelled by their self-generated flow and is non-zero only for $+1/2$ defects [27], μ is a mobility coefficient, $\boldsymbol{\zeta}_n^t$ and ζ_n^r are uncorrelated translational and rotational noises and $\boldsymbol{p}_n \cdot \boldsymbol{p}_n^\perp = 0$. In addition, $\boldsymbol{F}_n = -\nabla_{\boldsymbol{r}_n} F_{\rm F}$, where $F_{\rm F} = -4\pi^2 k \sum_{n\neq m} s_n s_m G(\boldsymbol{r}_n, \boldsymbol{r}_m) + 2\pi k \sum_n s_n \int {\rm d}A\, G(\boldsymbol{r}_n, \boldsymbol{r}) K(\boldsymbol{r})$, with $G(\boldsymbol{r}_n, \boldsymbol{r}_m)$ the Laplacian Green function on the torus [31], is the elastic force resulting from the inter-defect interactions and the interaction between the defects and the local Gaussian

curvature.

Eqs. (3) are solved numerically for fixed number of defects. Every time two oppositely charged defects come within a distance $r_c = 2a \times 10^{-3}$, representing the defect core radius, they annihilate and a new pair is created at a random position. Consistent with the outcome of our hydrodynamic simulations (Fig. 2d), the probability distribution for pair creation is chosen to be a linearly decreasing function of K, namely: $\rho_{\text{creation}} \sim 1 - b^2 K$ (up to normalization factors). We plot ρ_c , $n_\pm$ and the creation and annihilation rate densities obtained from an integration of Eqs. (3) in Fig. 3. Comparing with the hydrodyamic results in Fig. 2, we see remarkable agreement. As in our hydrodynamics simulations, the topological charge density ρ_c from the Coulomb gas model is monotonically increasing with the Gaussian curvature (Fig. 3b) and essentially unaffected by the system activity. Nevertheless, the number density of both positive and negative defects, $n_\pm$, is higher in the interior of the torus (Fig. 3c), in spite of the elastic interaction between the defects and the substrate forcing the $+1/2$ defects towards the exterior of the torus. The defects annihilation and creation rates match each other exactly and are increasingly larger in the region of negative K (Fig. 3d) as activity increases. Consistent with our hypothesis, a higher pair creation rate inside the torus leads to a larger density of positive defects in regions of negative Gaussian curvature, even though $\rho_c \sim K$. As elasticity driven-defect unbinding preferentially occurs in regions of vanishing Gaussian curvature [37] and is independent on activity, the origin of this process is ultimately hydrodynamical.

To further test the relevance of our theoretical predictions, we turn to experiments on microtubule-kinesin suspensions constrained to the surface of toroidal droplets [5, 39]. The kinesin motors are powered by 36 µM of adenosine triphosphate (ATP). In addition, we include an ATP regeneration system, phosphoenol pyruvate and pyruvate kinase/lactic dehydrogenase, and a depletant, polyethylene glycol (PEG), which causes the microtubules to assemble on the surface, where they form a nematic liquid crystal [31]. We then image the lower half of the toroidal droplet using confocal microscopy and project a region along the gravitational direction onto the plane (Fig. 4a). The local Gaussian curvature and $\boldsymbol{Q}$ are constructed using techniques from the computer vision literature [5]. We consider various regions on the surface of a given torus, calculate the mean Gaussian curvature in each region, $\langle K \rangle$, and correlate it with the time-averaged ρ_c and the time-averaged S in the region, as shown in Fig. 4b for the representative example toroid in Fig. 4a. We also consider the defect densities individually and correlate $n_\pm$ with $\langle K \rangle$ (Fig. 4c). Consistent with our theoretical results, we find that ρ_c and S depend linearly on $\langle K \rangle$ with a positive slope. In addition, we also observe that $n_\pm$ are linearly dependent on $\langle K \rangle$ with a negative slope, corresponding to a higher defect density in the interior of the toroidal droplet than on the exterior. Qualitatively, we observe this same behavior for a variety of toroids made with different aspect ratio and cross-sectional radius.

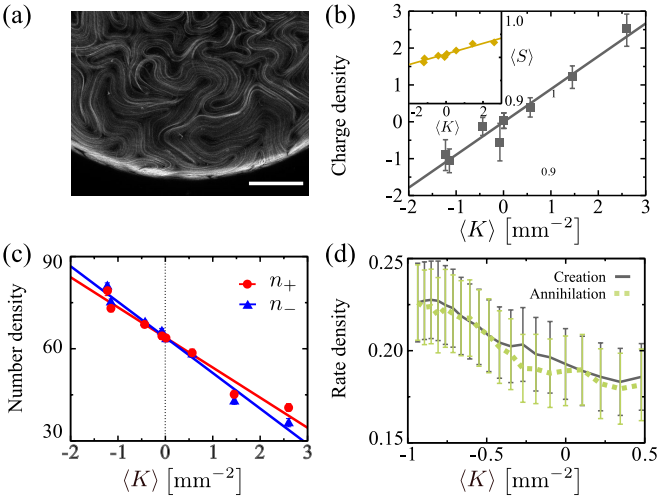

FIG. 4. Results from experiments with microtubules-kinesin suspensions. (a) Snapshot of the experiment. (b) Topological charge density and nematic order parameter (Inset). (c) Number density of $+1/2$ (red) and $-1/2$ (blue) disclinations. (d) Annihilation and creation rates. These results correspond to observations on a torus with aspect ratio 1.8 with minor radius 334 µm. The error bars in (b-d) correspond to the standard error of the mean. We note that the error in (c) is smaller than the plotted points. Scale bar in (a): 200 µm.

At the ATP concentration used in our experiments, $\boldsymbol{Q}$ evolves slowly enough to track the defects in time using a combinatorics-based particle tracking algorithm [40]. The individual trajectories for the $s = +1/2$ and $s = -1/2$ defects allow us to determine the creation and annihilation events; we consider the beginning and ending of a single trajectory as one-half of a defect creation or annihilation event, respectively. We then divide the number of creation and annihilation events in a region by its area and the total time of the experiment to get the creation and annihilation rate density. We find that these rates are equivalent and that they are larger in regions of negative $\langle K \rangle$ than in regions with positive $\langle K \rangle$, in agreement with the theoretical results. This is shown in Fig. 4d for the toroid in Fig. 4a. This agreement occurs without any dependence on the extrinsic curvature ($k_e = 0$) or explicit coupling between S and K ($k_{24} = 0$), highlighting the primary role of the intrinsic geometry and of the hydrodynamics.

In summary, we have introduced a generalization of the hydrodynamic theory of active nematics to arbitrarily curved sufaces. We applied this generalization to the specific case of an extensile active nematic on the surface of a torus and probed the effect of the substrate Gaussian curvature on the active nematic. Thanks to a combination of numerical simulations and experiments we have

established that the structure of the nematic phase is controlled by the substrate curvature in a twofold way. First, the activity-induced hydrodynamic unbinding of defect pairs is enhanced by curvature, leading to non-uniform nematic order and defect number density. Second, the passive elastic interactions between the defects and the underlying substrate geometry tends to bias the topological charge in regions of like-sign Gaussian curvature. We emphasize that the hydrodynamic approach developed here is general and applicable to situations other than that we have focused in this work.

We would like to thank Piermarco Fonda and Gareth Alexander for helpful discussions while producing this work. This work was supported by the Netherlands Organization for Scientific Research (NWO/OCW), as part of the Frontiers of Nanoscience program and the Vidi scheme (DJGP, LG), by the National Science Foundation (NSF 1609841) and the FLAMEL program (NSF 1258425) (PWE, AFN). We thank the Brandeis biological materials facility (NSF MRSEC DMR-1420382) for providing the materials for the experimental system used in this work.

* alberto.fernandez@physics.gatech.edu
† giomi@lorentz.leidenuniv.nl

[1] T. Surrey, F. Nedelec, S. Leibler, E. Karsenti, Science **292**, 1167 (2001).
[2] T. Sanchez, D. N. Chen, S. J. DeCamp, M. Heymann, Z. Dogic, Nature **491**, 431 (2012).
[3] Y. Sumino, K. H. Nagai, Y. Shitaka, D. Tanaka, K. Yoshikawa, H. Chaté, K. Oiwa, Nature **483**, 448 (2012).
[4] F. C. Keber, E. Loiseau, T. Sanchez, S. J. DeCamp, L. Giomi, M. J. Bowick, M. C. Marchetti, Z. Dogic, and A. R. Bausch, *Science* **345**, 1135 (2014).
[5] P. W. Ellis, D. J. G. Pearce, Y.-W. Chang, G. Goldsztein, L. Giomi, A. Fernandez-Nieves, Nat. Phys. **14**, 85 (2018).
[6] S. J. DeCamp, G. S. Redner, A. Baskaran, M. F. Hagan, Z. Dogic, Nat. Mater. **14**, 1110 (2015).
[7] P. Guillamat, J. Ignés-Mullol, F. Sagués, Proc. Natl. Acad. Sci. U.S.A. **113**, 5498 (2016).
[8] , P. Guillamat, J. Ignés-Mullol, F. Sagués, Nat. Commun. **8**, 564 (2017).
[9] V. Schaller, C. Weber, C. Semmrich, E. Frey, A. R. Bausch, Nature **467**, 72 (2010).
[10] V. Schaller, and A. R. Bausch, Proc. Nat. Acad. Sci. U.S.A. **110**, 4488 (2013).
[11] C. Dombrowski, L. Cisneros, S. Chatkaew, R. E. Goldstein, and J. O. Kessler, Phys. Rev. Lett. **93**, 098103 (2004).
[12] C. W. Wogelmuth, Biophys. J. **95**, 1564 (2008).
[13] H. P. Zhang, A. Beer, E.-L. Florin, H. L. Swinney, Proc. Natl. Acad. Sci. U.S.A. **107**, 13626 (2010).
[14] H. H. Wensink, J. Dunkel, S. Heidenreich, K. Drescher, R. E. Goldstein, H. Löwen, and J. M. Yeomans, Proc. Natl. Acad. Sci. U.S.A. **109**, 14308 (2012).
[15] J. Dunkel, S. Heidenreich, K. Drescher, H. H. Wensink, M. Bär, and R. E. Goldstein, Phys. Rev. Lett. **110**, 228102 (2013).
[16] H. Wioland, E. Lushi, R. E. Goldstein, New J. Phys. **18** 075002 (2016).
[17] I. H. Riedel, K. Kruse, J. A. Howard, Science **309**, 300 (2005).
[18] A. Creppy, O. Praud, X. Druart, P. L. Kohnke, F. Plouraboué, Phys. Rev. E **92**, 032722 (2015).
[19] S. Zhou, A. Sokolov, O. D. Lavrentovich, and I. S. Aranson, Proc. Nat. Acad. Sci. U.S.A. **111**, 1265 (2014).
[20] S. Shankar, M. J. Bowick, M. C. Marchetti, Phys. Rev. X **7**, 031039 (2017).
[21] R. Green, J. Toner, and V. Vitelli Phys. Rev. Fluids 2, 104201 (2017).
[22] R. Sknepnek, S. Henkes, Phys. Rev. E **91**, 022306 (2015).
[23] R. Zhang, Y. Zhou, M. Rahimi, J. J. de Pablo Nat. Commun. **7**, 13483 (2016).
[24] D. Khoromskaia, G. P. Alexander New J. Phys, **19**, 103043 (2017).
[25] O. Mickelin, J. Słomka, K. J. Burns, D. Lecoanet, G. M. Vasil, L. M. Faria, and J. Dunkel, Phys. Rev. Lett. **120**, 164503 (2018).
[26] L. Giomi, M. J. Bowick, X. Ma, M. C. Marchetti, Phys. Rev. Lett. **110**, 228101 (2013).
[27] L. Giomi, M. J. Bowick, P. Mishra, R. Sknepnek, M. C. Marchetti, Phil. Trans. R. Soc. A **372**, 20130365 (2014).
[28] S. Shankar, S. Ramaswamy, M. C. Marchetti, M. J. Bowick, Phys. Rev. Lett. **121**, 108002 (2018).
[29] M. J. Bowick, L. Giomi, Adv. Phys. **58**, 449 (2009).
[30] A. M. Turner, V. Vitelli, D. R. Nelson, Rev. Mod. Phys. **82**, 1301 (2010).
[31] See Supplemental Material at ...
[32] S. Kralj, R. Rosso, E. G. Virga, Soft Matter **7**, 670 (2011).
[33] G. Napoli, L. Vergori, Phys. Rev. Lett. **108**, 207803 (2012).
[34] G. Napoli, L. Vergori, Phys. Rev. E **85**, 061701 (2012).
[35] D. Jesenek, S. Kralj, R. Rosso, E. G. Virga, Soft Matter **11**, 2434 (2014).
[36] L. Giomi, Phys. Rev. X **5**, 031003 (2015).
[37] M. J. Bowick, D. R. Nelson, A. Travesset, Phys. Rev. E **69**, 041102 (2004).
[38] D. Jesenek, S. Kralj, R. Rosso, E. G. Virga, Soft Matter **11**, 2434 (2015).
[39] E. Pairam, H. Le, A. Fernandez-Nieves, Phys. Rev. E **90**, 021002(R) (2014).
[40] J. Crocker, D. Grier, J. Colloid Interface Sci. **179**, 298 (1996).